Available online at www.sciencedirect.com
ScienceDirect
Journal of the European Ceramic Society xxx (2014) xxx–xxx
www.elsevier.com/locate/jeurceramsoc

Short Communication

Surface textured $Sm_{0.5}Sr_{0.5}CoO_{3-\delta}$ as light absorber for solar thermoelectric generator

Zhenggang Fang [a], Chunhua Lu [a,*], Dongshan Gao [a], Yi Lu [a], Chaopeng Guo [a], Yaru Ni [a], Zhongzi Xu [a,**], Peiwen Li [b]

[a] State Key Laboratory of Materials-Oriented Chemical Engineering, College of Materials Science and Engineering, Nanjing Tech University, Nanjing 210009, PR China

[b] Department of Aerospace and Mechanical Engineering, The University of Arizona, Tucson, AZ 85721, United States

Received 6 August 2014; received in revised form 28 September 2014; accepted 6 October 2014

Abstract

Surface textured $Sm_{0.5}Sr_{0.5}CoO_{3-\delta}$ oxide ceramics were prepared by means of compression molding followed by high temperature sintering. The effects of surface texture on the optical and photo-thermal conversion performances of $Sm_{0.5}Sr_{0.5}CoO_{3-\delta}$ were investigated. Results showed that the solar absorptance of $Sm_{0.5}Sr_{0.5}CoO_{3-\delta}$ increased from 0.69 to 0.85 because of surface texturization. Besides, textured $Sm_{0.5}Sr_{0.5}CoO_{3-\delta}$ exhibited better photo-thermal conversion ability than the planar ones, with almost no selectivity to the incident irradiation, normal or oblique. Optimized samples were tested as sunlight absorber for concentrating solar thermoelectric generator. It is anticipated that the textured $Sm_{0.5}Sr_{0.5}CoO_{3-\delta}$ ceramic absorber can be extended to design non-tracking concentrating solar thermoelectric generators.

Keywords: $Sm_{0.5}Sr_{0.5}CoO_{3-\delta}$; Surface texture; Solar absorber; Solar thermoelectric generator

1. Introduction

Efficient utilization of solar energy is an applicable approach to cover the energy demand of human beings when the shortage of fossil fuels is gradually becoming a serious problem.[1–3] Among the various solar energy utilization technologies, the most prevalent ones are solar photovoltaic and solar thermal.[4] Unlike solar photovoltaic, which is restricted by the working wavelength above the band-gap, solar thermal technology utilizes a larger portion of the solar energy spectrum.[5] The traditional solar thermal power generation systems, such as a concentrated solar power (CSP) plant, uses mechanical heat engines to generate electric power; while solar thermoelectric generators (STEGs) are solid state heat engines that convert solar thermal to electric power based on the Seebeck effect.[6] To convert solar energy into electricity with high efficiency, a common challenge in CSP plants and STEGs is to achieve a high operating temperature.[6,7] In order to achieve this goal, optical concentration systems are used to focus or concentrate direct solar radiation, thereby increasing the energy flux. Meanwhile, the solar absorber should effectively convert the concentrated solar radiation into heat, and simultaneously lose little heat to the environment via thermal radiation. Spectrally selective absorber with high absorbance in the solar spectrum wavelengths ($\lambda < 2.5\ \mu m$) and low emissivity in the IR region may meet the performance requirement.[8] Currently, the operational temperatures of commercially available spectrally selective absorber materials are usually less than 800 K,[9,10] due to oxidation, interfacial diffusion and thermal degradation. To overcome these problems, the present study explored different materials and properties.

The materials known for high temperature solar absorbers include alumina (Al_2O_3),[11] silicon carbide (SiC),[12] carbide and boride ultra-high temperature ceramics.[13–15] Although Al_2O_3

* Corresponding author. Tel.: +86 25 83587252; fax: +86 25 83587220.
** Corresponding author. Tel.: +86 25 83172128; fax: +86 25 83172128.
E-mail addresses: chhlu@njtech.edu.cn (C. Lu), zzxu@njtech.edu.cn (Z. Xu).

http://dx.doi.org/10.1016/j.jeurceramsoc.2014.10.006
0955-2219/

and SiC exhibit good oxidation resistance and high thermal stability, they do not show excellent spectral selectivity because of low sunlight absorption of Al_2O_3 and high thermal emittance of SiC.[14] Carbide and boride ultra-high temperature ceramics show better spectral selectivity as compared to Al_2O_3 and SiC, however, they may only be operated in vacuum or under inert atmosphere, especially at high temperature.[13,14]

$Sm_{0.5}Sr_{0.5}CoO_{3-\delta}$ (SSC5) perovskite-type oxide is commonly considered as one of the most promising cathode materials for intermediate-temperature (500–800 °C) solid oxide fuel cell because of its good electrochemical performance and thermal stability.[16] Recently, we have studied the optical property and infrared emissivity of Sr-incorporated $Sm_{1-x}Sr_xCoO_{3-\delta}$ ($0.1 \le x \le 0.9$).[17] It was found that SSC5 exhibited the lowest infrared emissivity (0.25), however, it also showed the highest spectral reflectivity in the wavelength range of 0.3–2.5 μm. Considering that the spectral absorbance can be enhanced by textural effects without increasing the thermal emittance,[18] it is therefore advantageous to utilize surface texturing technology to tailor the absorbance and thus optimize the solar thermal conversion efficiency.

In this study, we demonstrate that the spectral absorbance of SSC5 can be enhanced by the introduction of the inverted quadrangular frustum-pyramid (or rectangular pyramid) cavities. In particular, the absorbance can be tailored by the geometric parameters of the cavities. The samples with surface texture have better photo-thermal conversion ability than the ones without, and therefore are selected as solar absorber for STEGs. Our study shows that textured SSC5 is a promising high-temperature solar absorber that may promote the application of STEGs in large scale.

2. Experimental procedure

2.1. Sample preparation

SSC5 precursor powder was prepared by the conventional solid-state reaction as described elsewhere.[17] After calcinations at 900 °C for 6 h, the obtained powder was ground and screened through a 200-mesh sieve.

To do tape casting, the SSC5 precursor powders were firstly mixed with the solvent (a mixture of 31 wt% ethanol, 56 wt% isopropanol and 13 wt% xylene) and the dispersant (castor oil) by ball milling for 4–6 h. Subsequently, the binder (polyvinyl butyral, M_w = 40,000–70,000) and the plasticizer (dibutyl phthalate) were added, and the mixture was remixed for 20–24 h. The mass fraction of the precursor powders, solvent, dispersant, binder and plasticizer were 63%, 28%, 1.5%, 5%, and 2.5%, respectively. The obtained slurry was degassed and casted onto a siliconed mylar carrier film. After drying at room temperature for 24 h, the green sheets with 120 μm in thick can be easily tailored and handled.

The surface textures were fabricated by means of compression molding, and the schematic diagram of fabrication process was illustrated in Fig. 1a. Firstly, the mold with a rectangular pyramid (or quadrangular frustum-pyramid) surface texture was pre-sprayed with a thin layer of paraffin. Thereafter, the green sheets were tailored into disks and stacked on the surface of mold layer by layer. Subsequently, these green sheets were pressed into discs with surface texture under 100 Mpa. Finally, the mold was heated to the melting temperature of the paraffin quickly, and the green compact could be easily peeled off. As a comparison, a planar sample was also fabricated.

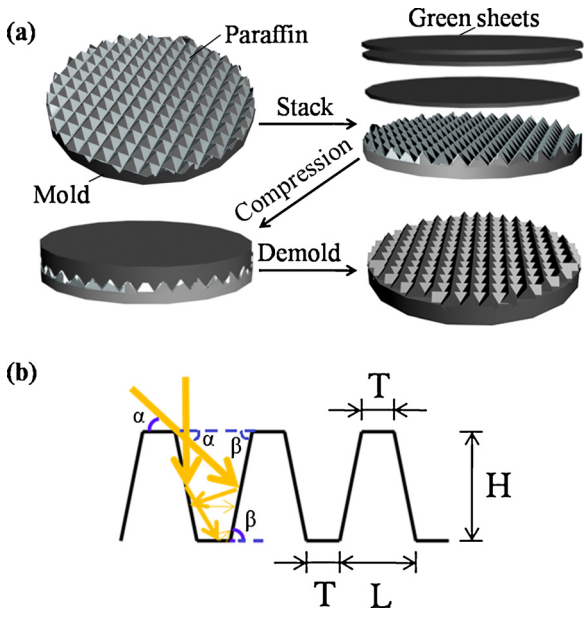

Fig. 1. (a) Schematic illustration of the fabrication of surface textures. (b) A cross-sectional view of the quadrangular frustum-pyramid.

Firstly, the green compacts were heated from room temperature to 450 °C at a heating rate of 1.5 °C/min, and held at 450 °C for 4 h to remove the organic materials. Thereafter, the furnace temperature was heated to 1230 °C at a heating rate of 3 °C/min. The samples were held at 1230 °C for 10 h.

2.2. Characterization

The morphologies were characterized by stereoscopic microscopy (ZSM 745T, Nikon). Reflectance spectra in the 200–2500 nm wavelength range were measured on a UV–vis–NIR spectrophotometer (Shimadzu UV-3101PC) with $BaSO_4$ as the reflectance sample.

To conduct photo-thermal measurements, a solar simulator (model 94043A, 4 × 4 in. source diameter, Newport) with an AM1.5 direct filter was used as the light source. The Fresnel lens was used for optical concentration. The optical power density was measured by a Hand-Held Optical Power/Energy Meter (model 1918-R, Newport) equipped with a Thermopile Detector (Model 818P-020-12, Newport). Temperatures of the samples were measured under the concentrated light irradiation at different time intervals using a surface thermocouple (NR-81533B, KREVOR).

For electrical measurement, a thermoelectric generator (TEG) module (TEP 1-1263-3.4, Thermonamic Electronics Corp., Ltd., China) was adhered between the ceramic absorber and a home-made water cooler with the thermally conductive

Please cite this article in press as: Fang Z, et al. Surface textured $Sm_{0.5}Sr_{0.5}CoO_{3-\delta}$ as light absorber for solar thermoelectric generator. *J Eur Ceram Soc* (2014), http://dx.doi.org/10.1016/j.jeurceramsoc.2014.10.006

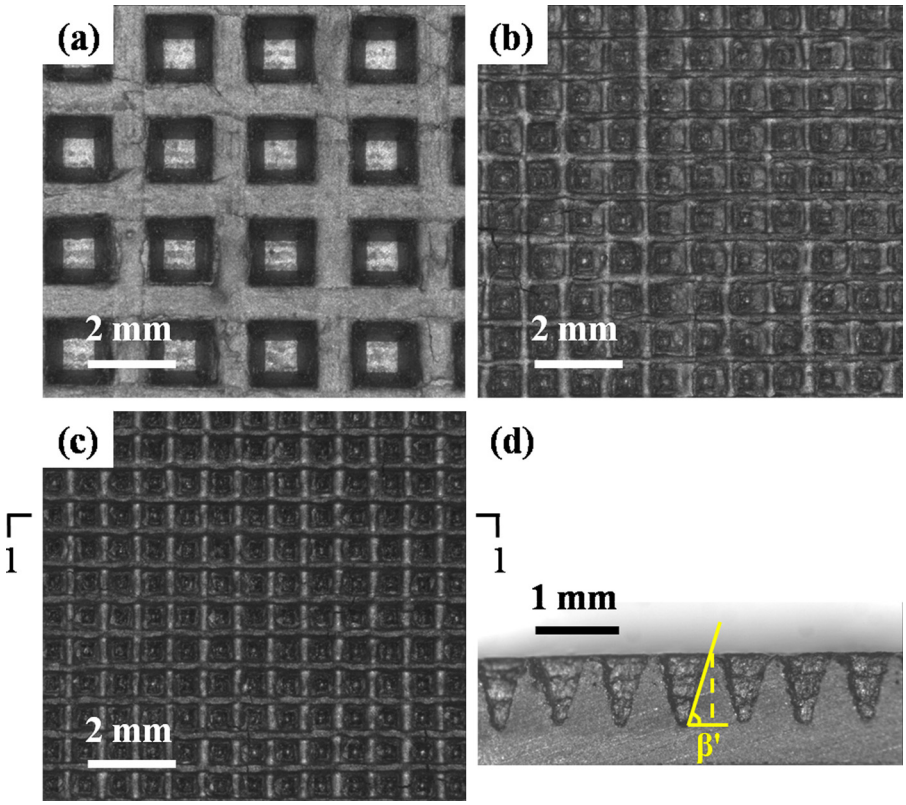

Fig. 2. Optical microscopy images of (a) SSC5-R242, (b) SSC5-R011, (c) SSC5-R012, and (d) an enlargement of "1–1" profile from (c).

adhesives. The current–voltage curves were measured with a sourcemeter (Keithley 2440 5A) controlled by a computer.

3. Results and discussion

In order to improve the light-harvesting performance of SSC5, textured surfaces with various shapes and different geometrical parameters were designed and prepared using compression molding technology (Fig. 1a). Paraffin was utilized as the release agent. The inverted quadrangular frustum-pyramid and inverted rectangular pyramid cavities were fabricated from their metal molds. In practice, the incidence of the incoming solar radiation may be perpendicular, or slanted with a certain incidence angle (α) (Fig. 1b). To effectively capture the light, the bevel angle (β) should be large enough to make the propagation direction of the first reflected light point down to the inner of the cavity. Generally, the minimum incidence angle is assumed to be 30° during the daylight (8:00 am to 4:00 pm).[19] Whereas the critical condition is $\alpha = 30°$ and also it is required that ($\alpha + \beta$) should be larger than 90° to keep reflected light always going forward; therefore, the angle β should be larger than 60°. The geometrical parameters of the quadrangular frustum-pyramid (or rectangular pyramid) including the frustum-pyramid length (T), base length (L), and frustum-pyramid height (H) are designed to meet the requirements of the bevel angle (Table 1).

Fig. 2 shows the optical micrographs of the as-prepared textured surfaces. The inverted quadrangular frustum-pyramid cavities (Fig. 2a) and inverted pyramid cavities (Fig. 2b and c) are formed on SSC5 with the geometrical parameters less than those of the molds due to the sintering shrinkage. Nevertheless, the bevel angle barely changed. For instance, the SSC5-R012 exhibits a bevel angle (β') of ~71° (Fig. 2d), which is approximately equal to the β of the corresponding mold (Table 1), indicating that the similar duplications of the mold structures are obtained.

Table 1
Characteristic geometrical parameters of the quadrangular frustum-pyramid and rectangular pyramid.

Surfaces	Abbreviations	T (mm)	L (mm)	H (mm)	β (°)
Planar	SSC5-P	–	–	–	–
Rectangular pyramid	SSC5-R242	2	4	2	63
	SSC5-R011	0	1	1	63
	SSC5-R012	0	1	2	72

The diffuse reflectance spectra of the samples under investigation are presented in Fig. 3. It can be clearly observed that the textured SSC5 have a lower reflectance as compared with the planar SSC5. Among all the textured surfaces, SSC5-R012 exhibits the lowest reflectance. The solar absorbance (α_S) can be derived from the reflectance spectrum according to the equation[20]:

$$\alpha_S = \frac{\int_{0.3\,\mu m}^{2.5\,\mu m}[1 - R(\lambda)]P_{Sun}(\lambda)d\lambda}{\int_{0.3\,\mu m}^{2.5\,\mu m} P_{Sun}(\lambda)d\lambda} \quad (1)$$

where λ is the wavelength, $R(\lambda)$ is the reflectance, $P_{Sun}(\lambda)$ refers to the normal solar irradiance at wavelength λ, which is defined according to ISO standard 9845-1 (1992), AM 1.5. The solar absorbance is calculated to be 0.69, 0.79, 0.82 and 0.85 for

Please cite this article in press as: Fang Z, et al. Surface textured $Sm_{0.5}Sr_{0.5}CoO_{3-\delta}$ as light absorber for solar thermoelectric generator. *J Eur Ceram Soc* (2014), http://dx.doi.org/10.1016/j.jeurceramsoc.2014.10.006

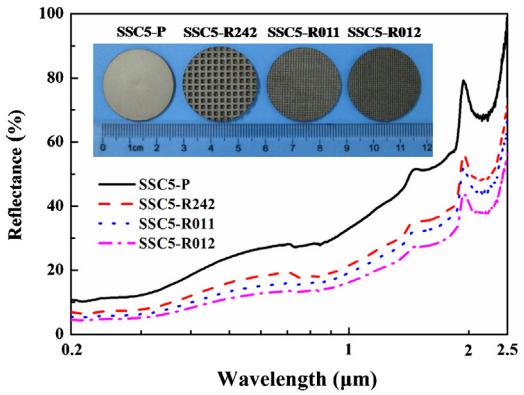

Fig. 3. Reflection spectra of the planar and textured SSC5 samples. The inset shows the photographs of these samples.

the SSC5-P, SSC5-R242, SSC5-R011 and SSC5-R012, respectively. In addition, the color appearance of the samples changes from light gray to dark gray with the increment of absorbance (see Fig. 3 inset). It is noteworthy that the intrinsic absorbance of SSC5 (0.69) is higher than that of carbide and boride ceramics, and the textured SSC5 shows higher absorbance than that of SiC.[13,14] As depicted in Fig. 1b, the higher absorption coefficient is obtained by multiple reflections.

The photo-thermal conversion performances of the planar and textured SSC5 were investigated by recording the temperature change of these materials under the concentrated light irradiation at different time intervals. Samples with the same weight were chosen for the measurement to ensure comparability of results. As shown in Fig. 4a, under the irradiation of concentrated light, the temperatures of SSC5-P increased rapidly. With the increase of incident fluxes, the temperature increase rate accelerated. Within 10 min the temperature changes (ΔT) of all the samples reached at a plateau and the equilibrium values increased with the incident fluxes. The ΔT of the textured SSC5 showed a similar manner in comparison with that of SSC5-P as the irradiation time and incident fluxes increased. Nonetheless, the temperature increase rate and the equilibrium values of SSC5-R012 are higher than those of SSC5-P (Fig. 4b), indicating that SSC5-R012 can convert light energy into heat more efficiently.

Notably, the above photo-thermal conversion measurements were all performed with normal incident irradiation. In practical applications, the optical concentration system usually needs to be installed with either single- or dual-axis tracking systems to track the path of the sun, which adds extra cost and complexity. Recently, the dome-shaped Fresnel lenses have been explored for broad-angle light concentrating,[21] which will contribute to fabricating static non-tracking solar concentrator. However, the concentrated light may irradiate on the absorber with an oblique angle of incidence.[22] So it is necessary to investigate the angular-dependent photo-thermal conversion property of the samples. Fig. 4c compares the equilibrium temperatures of the planar and textured SSC5 under irradiation at 9 W/cm^2 with the irradiation angle ranging from 0 to 60°. Here, the angle of incidence 0° represents for the normal incident irradiation. It can be seen that

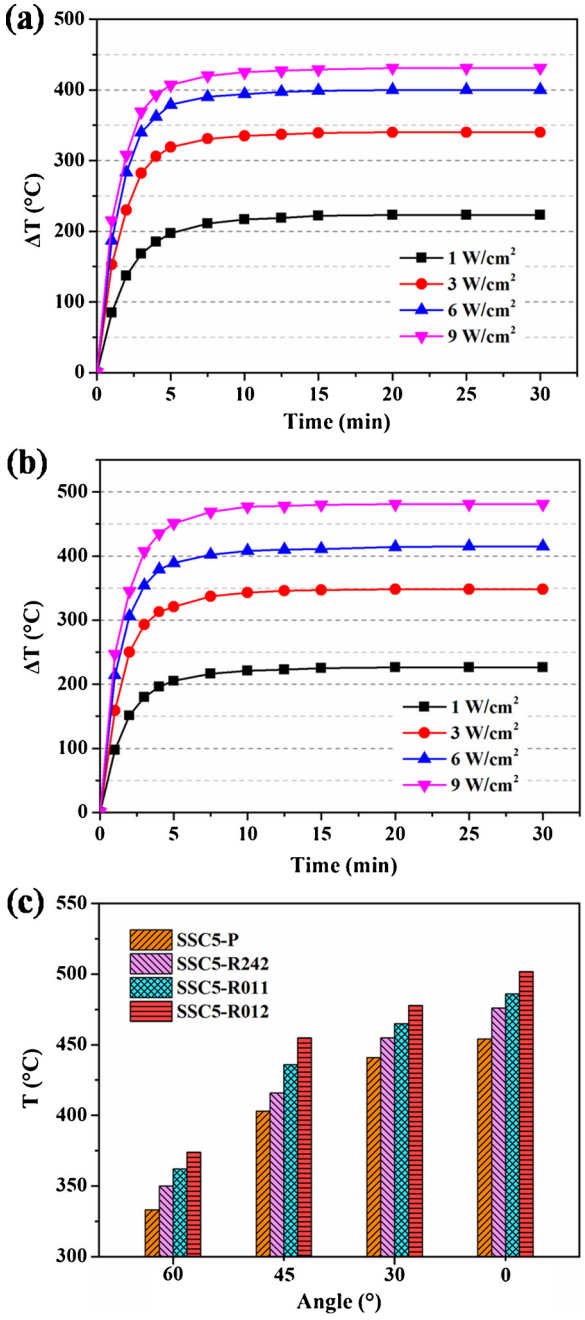

Fig. 4. Photo-thermal conversion performances of the planar and textured SSC5 under concentrated solar irradiation. Temperature change curves are given in (a) SSC5-P, (b) SSC5-R012 under irradiation at various incident fluxes, (c) Comparison of the equilibrium temperatures of SSC5-P and textured SSC5 samples under irradiation at 9 W/cm^2 with different irradiation angles.

the equilibrium temperatures decrease gradually with increasing irradiation angle, yet the textured SSC5 exhibit higher equilibrium temperatures than that of planar SSC5 for all the irradiation angles. SSC5-R012 shows the optimal photo-thermal conversion property. In the combination with the relationship between photo-thermal conversion temperatures and incident fluxes, it is reasonable to assume that a steady heat source can be obtained all day long by adjusting the optical concentration ratio of the dome-shaped Fresnel lenses.

Please cite this article in press as: Fang Z, et al. Surface textured $Sm_{0.5}Sr_{0.5}CoO_{3-\delta}$ as light absorber for solar thermoelectric generator. *J Eur Ceram Soc* (2014), http://dx.doi.org/10.1016/j.jeurceramsoc.2014.10.006

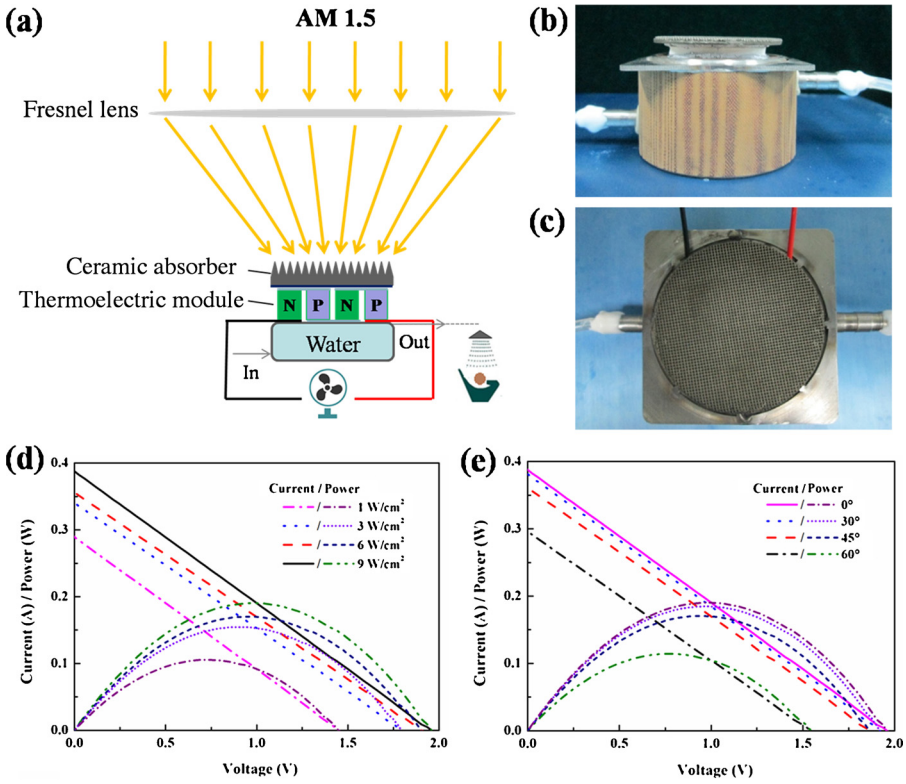

Fig. 5. (a) Illustration of a STEG device consists of optical collector, light absorber, thermoelectric module and cooling system. Photographs of the STEG device: (b) side view, (c) top view. (d) Current–voltage and power–voltage curves of the device under irradiation at various incident fluxes, (e) Current–voltage and power–voltage curves of the device under irradiation at 9 W/cm^2 with different irradiation angles.

SSC5-R012 was used as light absorber for STEGs. The experimental device, as illustrated in Fig. 5a, consists of an optical concentration system (Fresnel lens), ceramic absorber (SSC5-R012), thermoelectric module and cooling system. The thermoelectric module was sandwiched between the SSC5-R012 and a home-made water cooling system (Fig. 5b and c). A water cooling system is used because it can not only increase the temperature difference across the thermoelectric module, but also provide hot water which is necessary for daily life. To keep things simple, the water flux was set at 100 ml/min for all measurements. Current–voltage and power–voltage curves of the device under irradiation at various incident fluxes are shown in Fig. 5d. The nearly linear relationship of current and voltage indicates the generated voltage is constant.[23] Both the open circuit voltage (V_o) and short-circuit current (J_s) increased with the increment of incident fluxes (Fig. 5d), which show a similar manner as ΔT (Fig. 4b). The peak output power (P_{max}) is calculated to be 0.19 W for the device with an incident flux of 9 W/cm^2. The generated electricity can easily drive a propeller motor (see the video of the Supporting Information). In addition, 6 L hot water (42 °C) was obtained while the STEGs worked for an hour. The current–voltage characteristics of the STEGs under irradiation of 9 W/cm^2 with different irradiation angles were also tested (Fig. 5e). The V_o and J_s decreased with the increase of irradiation angles, which also show a similar manner as ΔT (Fig. 4c).

It is worth noting that the solar thermoelectric power conversion has not been fully exploited. For instance, convection losses were not eliminated under the experimental condition. This can be solved by enclosing the device inside the dome-shaped Fresnel lenses. Besides, the incident solar radiation power and the cooling water flux need to be further optimized according to the basic properties (figure of merit) of the thermoelectric module, which will be our future research subject.

4. Conclusions

We illustrated a facile compression molding technique for the fabrication of textured SSC5 ceramics. Benefiting from the textural effects, the solar absorbance of SSC5 increased from 0.69 to 0.85. Compared with the planar SSC5, the textured SSC5 showed better photo-thermal conversion ability no matter the incident irradiation was normal or oblique. The sample SSC5-R012 was used as light absorber for concentrating STEGs, which could generate electricity and hot water simultaneously. The experimental results in this work demonstrate that the SSC5 based light absorber makes the current design of non-tracking concentrating STEGs promising (Fig. S1).

Acknowledgments

This work was supported by the funding from the Priority Academic Program Development of the Jiangsu Higher Education Institutions (PAPD), the Innovation Foundation for Graduate Students of Jiangsu Province (CXZZ13_0425), the independent research topic of State Key Laboratory of

Materials-Oriented Chemical Engineering (ZK201211), the Key Laboratory of Inorganic Coating Materials, Chinese Academy of Sciences (KLICM-2014-10), as well as the Program for Changjiang Scholars and Innovative Research Team in University (PCSIRT, IRT1146).

Appendix A. Supplementary data

Supplementary data associated with this article can be found, in the online version, at http://dx.doi.org/10.1016/j.jeurceramsoc.2014.10.006.

References

1. Lewis N, Nocera D. Powering the planet: chemical challenges in solar energy utilization. *Proc Natl Acad Sci U S A* 2006;**103**:15729–35.
2. Roeb M, Neises M, Monnerie N, Sattler C, Pitz-Paal R. Technologies and trends in solar power and fuels. *Energy Environ Sci* 2011;**4**:2503–11.
3. Tian Y, Zhao CY. A review of solar collectors and thermal energy storage in solar thermal applications. *Appl Energy* 2013;**104**:538–53.
4. Baranowski LL, Snyder GJ, Toberer ES. Concentrated solar thermoelectric generators. *Energy Environ Sci* 2012;**5**:9055–67.
5. Guo CF, Sun TY, Cao F, Liu Q, Ren ZF. Metallic nanostructures for light trapping in energy-harvesting devices. *Light Sci Appl* 2014;**3**:e161.
6. Kraemer D, Poudel B, Feng HP, Caylor JC, Yu B, Yan X, et al. High-performance flat-panel solar thermoelectric generators with high thermal concentration. *Nat Mater* 2011;**10**:532–8.
7. Romero M, Steinfeld A. Concentrating solar thermal power and thermochemical fuels. *Energy Environ Sci* 2012;**5**:9234–45.
8. Kennedy CE. *Review of mid- to high-temperature solar selective absorber materials, NREL/TP-520-31267*. Colorado: National Renewable Energy Laboratory; 2002, July.
9. Liu Y, Wang C, Xue YF. The spectral properties and thermal stability of NbTiON solar selective absorbing coating. *Sol Energy Mater Sol Cells* 2012;**96**:131–6.
10. Rinnerbauer V, Lenert A, Bierman DM, Yeng YX, Chan WR, Geil RD, et al. Metallic photonic crystal absorber–emitter for efficient spectral control in high-temperature solar thermophotovoltaics. *Adv Energy Mater* 2014:1400334.
11. Karni J, Kribus A, Rubin R, Doron P. The "porcupine": a novel high-flux absorber for volumetric solar receivers. *J Sol Energy Eng* 1998;**120**:85–95.
12. Agrafiotis CC, Mavroidis I, Kostandopoulos AG, Hoffschmidt B, Stobbe P, Fernandez M, et al. Evaluation of porous silicon carbide monolithic honeycombs as volumetric receivers/collectors of concentrated solar radiation. *Sol Energy Mater Sol Cells* 2007;**91**:474–88.
13. Sani E, Mercatelli L, Sansoni P, Silvestroni L, Sciti D. Spectrally selective ultra-high temperature ceramic absorbers for high-temperature solar plants. *J Renew Sustain Energy* 2012;**4**:033104.
14. Sciti D, Silvestroni L, Mercatelli L, Sans J-L, Sani E. Suitability of ultra-refractory diboride ceramics as absorbers for solar energy applications. *Sol Energy Mater Sol Cells* 2013;**109**:8–16.
15. Sciti D, Silvestroni L, Sans J-L, Mercatelli L, Meucci M, Sani E. Tantalum diboride-based ceramics for bulk solar absorbers. *Sol Energy Mater Sol Cells* 2014;**130**:208–16.
16. Guo YM, Chen DJ, Shi HG, Ran R, Shao ZP. Effect of Sm^{3+} content on the properties and electrochemical performance of $Sm_xSr_{1-x}CoO_3$ ($0.2 \leq x \leq 0.8$) as an oxygen reduction electrodes on doped ceria electrolytes. *Electrochim Acta* 2011;**56**:2870–6.
17. Chen L, Lu CH, Fang ZG, Lu Y, Ni YR, Xu ZZ. Variable infrared emittance of Sr-incorporated $Sm_{1-x}Sr_xCoO_3$ ($0.1 \leq x \leq 0.9$). *J Phys D Appl Phys* 2013;**46**:105302.
18. Bogaerts WF, Lampert CM. Materials for photothermal solar energy conversion. *J Mater Sci* 1983;**18**:2847–75.
19. Yu R, Ching K-L, Lin QF, Leung S-F, Arcrossito D, Fan ZY. Strong light absorption of self-organized 3-D nanospike arrays for photovoltaic applications. *ACS Nano* 2011;**5**:9291–8.
20. Mastai Y, Polarz S, Antonietti M. Silica-carbon nanocomposites: a new concept for the design of solar absorbers. *Adv Funct Mater* 2002;**12**:197–202.
21. Akisawa A, Hiramatsu M, Ozaki K. Design of dome-shaped non-imaging Fresnel lenses taking chromatic aberration into account. *Sol Energy* 2012;**86**:877–85.
22. O'Neill MJ, Mcdanal AJ, Perry JL. *Development of a Fresnel lens gallium arsenide photovoltaic concentrator for space applications, Phase II Final Report, NASA SBIR Contract No. NAS3-25192*; 1990, October.
23. Chen YQ, Chen KW, Bai H, Li L. Electrochemically reduced graphene porous material as light absorber for light-driven thermoelectric generator. *J Mater Chem* 2012;**22**:17800–4.